26th International Congress on Modelling and Simulation, Adelaide, SA, Australia, 30 Nov–4 Dec 2025
mssanz.org.au/modsim2025

Optimising port–hinterland container transportation for resilience and sustainability

L Mennecke [a], J Pannek [a], M Papini [b]

[a]Institute for Intermodal Transport and Logistics Systems, Hermann-Blenk-Str.42, 38108 Braunschweig, Germany
[b]School of Information and Physical Sciences, University Dr, Callaghan, Newcastle, 2308, NSW, Australia

Abstract: Port–Hinterland Container Transportation Networks (PHCTNs) are critical infrastructures for global trade, enabling the inland distribution of maritime cargo. As schematically illustrated in Figure 1, these systems consist of a central port connected via multimodal transport corridors (road and rail) to inland hubs and hinterland destinations. However, PHCTNs face growing vulnerabilities due to climate change-related disruptions (CCDs), such as floods, bushfires, and cyclones. These events can severely limit network functionality by damaging nodes and routes, particularly when they affect both seaport and inland infrastructure. Ensuring operational continuity under such disruptions while limiting environmental impact presents a pressing challenge for infrastructure and logistics planners. This paper introduces a novel two-stage optimization framework, the Resilient and Green PHCTN (RG-PHCTN), designed to support strategic decision-making for disruption response and sustainable recovery.

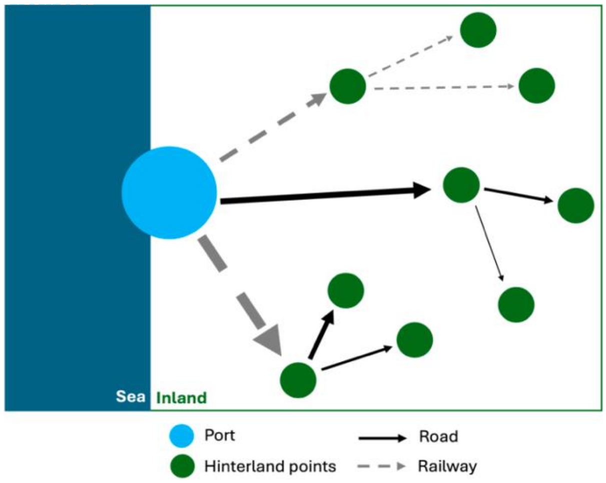

Figure 1 Example configuration of a Port-Hinterland Container Transportation Network

The RG-PHCTN integrates spatial disruption modelling, Monte Carlo simulation, and a sequential Mixed Integer Linear Programming (MILP) model that jointly optimizes recovery actions at both seaport and hinterland levels. The model evaluates and selects recovery strategies based on 3 dimensions: restoration time, implementation cost, and CO_2 emissions. Resilience is quantitatively defined as the ratio between containers successfully delivered after disruption and the total hinterland demand, providing a consistent metric across disruption types.

Computational experiments are conducted on a synthetic network based on the Port of Newcastle, Australia, with three connected dry ports. Stylised disruption scenarios represent CCDs and serve to illustrate the framework's functionality rather than provide precise forecasts. Over 900 Monte Carlo samples show that the model adapts recovery actions to disruption type, severity, and location. Bushfires—being spatially localized—result in high resilience (mean 0.93) and low CO_2 emissions (18 kg CO_2e/twenty-foot equivalent units), while widespread cyclones lead to lower resilience (0.82) and higher emissions (47 kg CO_2e/ twenty-foot equivalent units). The model robustly identifies high-performing recovery strategies, such as temporary seaport repairs and hinterland mode shifts, and demonstrates how these trade-offs vary across disruption scenarios.

This study offers a first-of-its-kind integration of resilience optimization and sustainability in port–hinterland networks. The RG-PHCTN provides a flexible and extensible decision-support tool for planners seeking to mitigate climate risks while minimizing environmental costs. Future extensions will incorporate data-driven disruption forecasting via machine learning, as well as a broader catalogue of granular recovery measures to improve realism and operational applicability.

Keywords: *Port-hinterland Container Transportation Network; Green Network Design Problem; Environmental Sustainability; Resilience*

1. INTRODUCTION

Container transportation between Australia's seaports and hinterlands is a cornerstone of national logistics and trade. In 2022–23, major Australian container ports handled over 8 million twenty-foot equivalent units (TEUs) (Bureau of Infrastructure and Transport Research Economics 2023), around 186 million tonnes and AUD 18 billion in value. With 0.33 TEUs moved per person for a population of 26 million, Australia's per capita throughput is more than double that of the U.S. (0.15 TEUs) (U.S. Bureau of Transportation Statistics 2025). These volumes are transported nationwide via Port–Hinterland Container Transport Networks (PHCTN).

Given their strategic locations and vital economic role, seaports and PHCTNs are highly exposed to climate-related disasters (Tian et. Al. 2024) such as cyclones and flooding. For example, in February 2025, Tropical Cyclone Zelia forced the closure of Port Hedland—Australia's largest iron ore port, halting exports and disrupting supply chains (Safe to Work 2025).

Becker et al. (2018) argue that enhancing port resilience requires actionable plans for implementing resilience measures, yet only a small share of international ports have adopted concrete strategies. While improving PHCTN resilience is crucial for maintaining operations during disruptions, this must be achieved with attention to environmental impacts, as port–hinterland transport significantly contributes to CO_2 emissions in the logistics chain (Liu et al. 2021). In response, this study introduces the Resilient and Green PHCTN (RG-PHCTN), an optimisation framework for developing environmentally sustainable and climate-resilient recovery plans for PHCTNs. The RG-PHCTN aims to enhance recovery from climate change-related disruptions (CCDs) while minimising CO_2 emissions from operations. We adopt the definition of resilience from Chen et al. (2017), describing a PHCTN's resilience as its capacity to maintain cargo flow and restore performance through recovery actions, within acceptable time and cost, when affected by climate change-related events.

We integrate spatially explicit disruption modelling with a two-stage Mixed Integer Linear Programming (MILP) framework that captures both seaport and hinterland recovery decisions under varying disruption scenarios. We conduct a series of computational experiments on a synthetic network based on the Port of Newcastle, Australia. These experiments use stylised data to systematically evaluate recovery performance across multiple disruption scenarios, illustrating how the framework enables quantitative comparison of resilience outcomes along economic and environmental dimensions.

2. THE RESILIENT AND GREEN PORT-HINTERLAND CONTAINER TRANSPORTATION NETWORK PROBLEM

According to Notteboom et al. (2022), a container port-hinterland refers to the inland area over which a port conducts its business, characterized by dispersed origins and destinations, competing ports, and typically unbalanced bi-directional flows. Within this context, a PHCTN can be understood as an intermodal network through which seaports coordinate container dispatches and shippers make transport choices across multiple modes (e.g., road, rail, and barge). This study focuses on RG-PHCTNs, which aims to make PHCTNs both resilient and green, aiming to enhance recovery capacity and minimize CO_2 emissions associated with operations.

We evaluate RG-PHCTN using the mathematical model combined with CCD scenarios based on the notation in Table 1. To quantify resilience under these CCDs, resilience must be expressed mathematically. We define Ξ as the set of all possible CCD scenarios. A particular scenario is denoted by ξ.We follow the definition of resilience presented in (Chen 2012), quantitatively expressed as:

$$\text{Resilience}(\xi) = E\left(\frac{\text{TF}(\xi)}{(\sum_{\omega \in W} d_\omega)}\right) \tag{1}$$

where the resilience is the expected value of the ratio of the number of containers delivered post-disruption $TF(\xi)$ and the total dry port demand $\sum_{\omega \in W} d_\omega$. Values approaching 1 indicate strong resilience. We assume this ideal input-output ratio when no CCD has occurred.

Our mathematical formulation builds on the model introduced in (Chen et al. 2017) with a key modification to the objective function. Specifically, we extend their original formulation by incorporating an environmental dimension: minimizing the CO_2 emissions associated with the recovery actions, alongside recovery time and cost, to promote a more sustainable network response. This extension reflects growing recognition that resilience and environmental sustainability must be addressed jointly, particularly in sectors like port–hinterland transport, which contribute significantly to CO_2 emissions.

Table 1 Notation of parameters

Notation	Type	Description
Ξ	Set	Set of CCD scenarios
S		Set of seaports
W		Set of dry ports
K		Set of recovery activities in the hinterland

Notation	Type	Description
J		Set of recovery activities in the seaport
L		Set of links between seaports and dry ports
p	Parameter	Merchandise value per container [USD/TEU]
λ_s		Weighting factor for penalizing CO_2 emissions at the seaport $s \in S$ [h/kg CO_2]
λ_ω		Weighting factor for penalizing CO_2 emissions at the dry port $\omega \in W$ [USD/kg CO_2]
τ^{max}		Maximum delivery time (dry port to ship via seaport)
v_{0s}		Nominal operation rate at the seaport $s \in S$
$\delta_{c\omega}$		Binary damage indicator for dry port $\omega \in W$
$\delta_{l\omega}$		Binary damage indicator for link $l \in L$
δ_s		Binary damage indicator for seaport $s \in S$
τ_ω		Delivery time (post- CCD) to dry port $\omega \in W$
τ_s		Post-CCD operation time at seaport $s \in S$
$\Delta c_{\omega k}$		Capacity increase on dry port $\omega \in W$ via recovery action $k \in K$
$\Delta l_{\omega k}$		Capacity increase on link $l \in L$ via recovery action $k \in K$
Δc_{sj}		Capacity increase at seaport $s \in S$ via recovery action $j \in J$
$t_{\omega k}$		Operation time after recovery action $k \in K$ at dry port $\omega \in W$
t_{sj}		Operation time after recovery action $j \in J$ at seaport $s \in S$
$t^R_{\omega k}$		Implementation time of recovery action $k \in K$ at dry port $\omega \in W$
t^R_{sj}		Implementation time of recovery action $j \in J$ at seaport $s \in S$
$e_{\omega k}$		CO2-Emission of recovery action $k \in K$ at dry port $\omega \in W$ [kg CO_2]
e_{sj}		CO2-Emission of recovery action $j \in J$ at seaport $s \in S$ [kg CO_2]
$b_{\omega k}$		Cost of implementing recovery action $k \in K$ at dry port $\omega \in W$
b_{sj}		Cost of implementing recovery action $j \in J$ at seaport $s \in S$
b_s		Available recovery budget for seaport $s \in S$
d_ω		Demand at dry port $\omega \in W$
f_ω	Decision variable	Flow (delivered container volume) for dry port $\omega \in W$
$\gamma_{\omega k}$		Binary recovery decision of recovery action $k \in K$ at dry port $\omega \in W$
γ_{sj}		Binary recovery decision of recovery action $j \in J$ at seaport $s \in S$
$TF(\xi)$	Output	Total satisfied container flow for CCD scenario $\xi \in \Xi$

The mathematical formulation comprises 2 sequential MILP sub-models: the Seaport Disruption Response Model (Sub-model 1), which captures the seaport's recovery decisions, and the Hinterland Disruption Response Model (Sub-model 2), which describes shippers' operational adjustments. Notably, the 2 sub-models are interconnected through their mutual dependence on available infrastructure capacity. Sub-model 1 determines the limit of the throughput at the seaport, while Sub-model 2 determines the actual container flow demand arriving at the port. If the total dispatched flow exceeds the restored capacity, the system is bottlenecked at the seaport. Conversely, if hinterland disruptions dominate, the flow is constrained by dry port or transport link availability.

2.1. Seaport disruption response model

Representing the strategic decision-making of seaport terminal operators, the MILP model

$$\min_{\gamma_{sj}(\xi)} T_s(\xi) \quad = \tau_s(\xi) + \delta_s(\xi) \sum_j \left(\left(t_{sj}(\xi) - \tau_s(\xi) \right) \gamma_{sj}(\xi) \right) + \delta_s(\xi) \sum_j t^R_{sj}(\xi)\, \gamma_{sj}(\xi) + \delta_s(\xi) \lambda_s \sum_j e_{sj}(\xi)\, \gamma_{sj}(\xi) \tag{2}$$

Subject to

$$\sum_j b_{sj}(\xi) \gamma_{sj}(\xi) \le b_s(\xi), \quad \forall j \in J \tag{3}$$

$$b_s(\xi) = p \cdot \max\left\{0, \sum_\omega d_\omega - c_s(\xi)\right\} \tag{4}$$

$$\sum_j \gamma_{sj}(\xi) \le 1 \tag{5}$$

$$\gamma_{sj}(\xi) \in \{0,1\}, \quad \forall j \in J \tag{6}$$

minimizes the operation time at the seaport, which is defined in this study as the absolute duration required for the port to process its post-disruption container throughput, accounting for routine operating hours and any additional delays or extensions introduced by disruptions or recovery measures. In the context of the objective function (2), operation time incorporates baseline operating time after a disruption, decreased operating time after disruption due to recovery action, time required for implementing specific recovery actions, and a time-equivalent penalty reflecting the environmental impact (CO_2 emissions) of those actions. All operation times used in the objective function are absolute durations in hours, representing the total time needed to restore and maintain seaport operation post-disruption. All terms are additive and expressed in consistent units so that the total objective value accurately reflects trade-offs between faster recovery and lower environmental impact. Constraint (3) ensures that the implementation costs of the selected recovery action do not exceed the available recovery budget. Constraint (4) defines this budget endogenously as the economic loss resulting from undelivered containers due to the CCD, under the assumption that a recovery investment is only rational if it offsets this loss. Constraint (5) enforces the selection of exactly one recovery action, while Constraint (6) defines the decision variable as binary.

2.2. Hinterland disruption response model

After the seaport operators selected a recovery action, each shipper in the hinterland may decide (a) what recovery strategies to implement and (b) how many containers to dispatch to the seaport. To this end, we utilise the model

$$\min_{\gamma_{\omega k}(\xi), f_\omega(\xi)} TC_\omega(\xi) = \epsilon\left(\delta_{c\omega}(\xi) + \delta_{l\omega}(\xi) - 1\right) \sum_k b_{\omega k}(\xi)\gamma_{\omega k}(\xi) + p \cdot \left(d_\omega - f_\omega(\xi)\right) + \lambda_\omega e_{\omega k}(\xi)\, \gamma_{\omega k}(\xi x) \tag{7}$$

Subject to

$$f_\omega(\xi) \leq \min\left\{d_\omega, c_\omega(\xi) + \delta_{c\omega}(\xi) \sum_k \Delta c_{\omega k}\gamma_{\omega k}(\xi), l_\omega(\xi) + \delta_{l\omega}(\xi) \sum_k \Delta l_{\omega k}\gamma_{\omega k}(\xi)\right\} \tag{8}$$

$$\tau_\omega(\xi) + \epsilon(\delta_{c\omega}(\xi) + \delta_{l\omega}(\xi) - 1) \sum_k \left(t_{\omega k}(\xi) - \tau_\omega(\xi)\right)\gamma_{\omega k}(\xi) + \epsilon(\delta_{c\omega}(\xi) + \delta_{l\omega}(\xi) - 1) \sum_k t^R_{\omega k}(\xi)\gamma_{\omega k}(\xi) + \frac{f_\omega(\xi)}{v_{0s} \cdot \left(\frac{c_s(\xi)}{c_{s,0}}\right)} \leq \tau^{max} \tag{9}$$

$$\sum_k \gamma_{\omega k}(\xi) \leq 1, \quad \forall \omega \in W, k \in K \tag{10}$$

$$\gamma_{\omega k}(\xi) \in \{0,1\}, \quad \forall \omega \in W, k \in K \tag{11}$$

$$f_\omega(\xi) \geq 0 \tag{12}$$

The objective function (7) minimises the total cost incurred by hinterland shippers in response to a CCD scenario. This cost depends on the chosen recovery action at the dry port level as well as on the container flow, which is itself constrained by the recovery outcome determined in Sub-model 1. In this study, flow refers to the absolute volume of TEUs successfully delivered post-disruption, subject to infrastructure capacities and recovery actions. The total cost comprises 3 components: the selected recovery implementation cost, a penalty associated with unsatisfied demand, and a time-equivalent penalty accounting for the CO_2 emissions generated by the recovery action. $\epsilon(t)$ is a step function equal to 0 for $t < 0$ and 1 for $t \geq 0$, ensuring recovery cost in the hinterland are included only when the dry port, the link, or both are damaged. Constraint (8) defines the flow f_ω as the minimum of three values: the total demand at the dry port, the available capacity at the dry port after implementing recovery measures, and the available link capacity (e.g., via rail) post-recovery. This constraint ensures that physical capacity limits are respected. Constraint (9) enforces a delivery time restriction. The total time includes the post-CCD delivery time, the time savings induces by implementing the selected recovery action, the implementation time of the recovery, and the handling time at the seaport. The sum of these components must not exceed a predefined maximum delivery time, as delays beyond this threshold are assumed to incur significant economic penalties. Constraint (10) ensures that at most one recovery strategy can be selected for each dry port, while Constraint (11) defines the recovery decision variable as binary. Finally, Constraint (12) ensures that the container flow remains non-negative.

2.3. Total container flow and resilience calculation

To calculate the resilience measure, the total container flow $TF(\xi)$ delivered under scenario ξ must be determined. The total flow is defined as the minimum of 2 system-level quantities: (a) the cumulative container volume dispatched by hinterland shippers or (b) the handling capacity available at the seaport after the implementation of recovery actions. Formally, this is expressed as:

$$TF(\xi) = \min\left\{\sum_\omega f_\omega(\xi), c_s(\xi) + \delta_s(\xi) \sum_j \Delta c_{sj}\gamma_{sj}(\xi)\right\} \tag{13}$$

The first term is determined by the Hinterland-model 2, whereas the second term, is given by the decisions made in the Seaport-model. Each action contributes a specific increase in operational capacity depending on the damage state. By solving this integrated two-stage mathematical framework, we identify disruption-specific recovery strategies and flow coordination decisions that jointly contribute to building a resilient and green PHCTN.

3. COMPUTATIONAL RESULTS

3.1. Designed port-hinterland container transportation network

The study considers a synthetic PHCTN based on the Port of Newcastle and 3 associated dry ports. The network is fully connected, with each node pair linked by intermodal transport options and initial link capacities set at 100 %, assuming no pre-existing disruptions. Dry port locations were selected to represent plausible inland terminal positions at varying distances from the seaport, ensuring geographic dispersion across the hinterland. For simplicity, the layout is constructed using Euclidean distances between nodes to approximate transport costs but allows for direct Open Street Map integration.

3.2. Simulation Setup

To solve the two-stage MILP model, we follow a sequential process. Based on disruption scenarios representing CCDs, multiple independent Monte Carlo samples are generated by varying disruption type, location, and capacity loss values. For each sample seaport and hinterland models are solved sequentially to determine the optimal seaport recovery action as well as the optimal hinterland recovery action and resulting container flows, respectively. The resilience of each scenario is calculated, and the expected value of the resilience across samples is used to assess network performance and compare recovery strategies.

We evaluate the network performance under 3 CCD scenarios set in the Australian context: flooding, cyclone, and bushfire. These were selected based on Sims and Canadell (2024), who highlight that climate change is driving more severe heatwaves, longer fire seasons, and shifts toward intense rainfall events. Following Nair et al. (2010), each scenario is defined by epicentre, intensity, and network impact, with disruptions modelled probabilistically. Effects are represented as stylised capacity reductions and increased baseline operation times, capturing reduced efficiency during and after the event. Disruption impacts are computed based on Euclidean distances between disruption epicentre and network elements, applying the respective capacity loss factors.

Table 2 Climate change-related disruption scenarios

Scenario	Zone	Infrastructure	Capacity reduction	Operation time impact
Flooding	400m	Route (road or rail)	100% (unusable)	N/A
		Dry Port	100% (closed)	N/A
		Seaport	50 – 75%	1 – 8 × baseline
	400m – 1 km	Route	0 – 50%	1 – 5 × baseline
		Dry Port	0 – 50%	1 – 5 × baseline
		Seaport	0 – 50%	1 – 3 × baseline
Cyclone	800m	Route	100% (unusable)	N/A
		Dry Port	100% (closed)	N/A
		Seaport	50 – 75%	1 – 8 × baseline
	800m – 2km	Route	30 – 70%	2 – 6 × baseline
		Dry Port	30 – 70%	2 – 6 × baseline
		Seaport	0 – 50%	1 – 3 × baseline
Bushfire	200m	Route	100% (unusable)	N/A
		Dry Port	100% (closed)	N/A
		Seaport	50 – 75%	1 – 8 × baseline
	200 – 700m	Route	20 – 60%	1.5 – 4 × baseline
		Dry Port	20 – 50%	1 – 3 × baseline
		Seaport	0 – 40%	1 – 4 × baseline

Flooding scenarios apply an impact radius 400m around the epicentre. Road and rail in this area become unusable (100% loss), the dry port closes, and the seaport runs at 25–50% capacity with 1–8 times delays. In the 400m–1km buffer, route capacities decrease by 0–50%, operation times rise by 1–5 times, and dry ports face 0–50 % capacity loss. Seaport impacts in this zone are lighter (1–50 % capacity loss, up to 3 times delays). The cyclone scenario represents widespread coastal disruption within an 800 m radius. Inside this zone, transport infrastructure is unusable and dry ports are closed; seaports run at 25–50 % capacity with 1–8 times delays. In the 800m–2km buffer, routes and dry ports operate at 30–70 % capacity, with 2–6 times delays. The seaport has 1–50% capacity loss and 1–3 times longer operation times. Highly localised bushfire scenarios affect a 200m radius, where roads and rail are unusable, the dry port is closed, and the seaport operates at 25–50 % capacity with 1–8 times delays. In the 200–700m buffer, road capacities drop 20–60 %, operation times increase 1.5–4 times, and dry ports lose 20–50 % capacity with 1–3 times delays. The seaport remains operational with 1–40 % capacity loss and up to 4 times delays. The chosen values are synthetic but intended to reflect relative disruption scales and enable meaningful testing of model responses.

Based on the 3 disruption scenarios, recovery actions adopted from Chen et al. (2017) include 2 seaport and 3 hinterland strategies summarised in Table 3. Recovered capacity values show the percentage of baseline seaport or dry port capacity restored. Recovered operation and implementation times are given as percentages of the baseline operation time, reflecting relative durations compared to normal conditions.

Table 3 Possible recovery actions with associated gains

Recovery action	Recovered capacity (%)			Rec. operation time (%)	Impl. time (%)	Impl. cost ($)	CO2 Emissions (kg CO2e/TEU)
	Seaport	Dry port	Route				
(S1) Seaport: Redundant Resources	60	-	-	167	50	310,000	5
(S2) Seaport: Temporary Repair	80	-	-	125	150	696,980	40
(H1) Shippers: Alt. Dry Port + Rail	-					0	15
(H2) Shippers: Switch to Road	-	100	Real world data	20	20		70
(H3) Shippers: Wait for Repairs	-	80	80	100	100	0	0

3.3. Computational Experiments on designed network

The entire solution procedure is implemented in Python 3.10 using Jupyter Notebook for model coordination and output visualization. The MILP problems are formulated using the PuLP optimization library and solved with its default open-source solver (CBC). All simulations are performed on a MacBook Pro with an Apple M1 Pro chip, 16 GB RAM, running macOS Sequoia 15.5.

Using 300 samples for each scenario, the resilience and mean CO_2 emissions across all samples of the same scenario type were computed to assess the performance of each recovery strategy. The computational results are presented in Table 4.

Table 4 Computational Results on the design PHCTN

Scenario	Resilience(ξ)	Mean CO_2 Emissions (kg CO_2 e/TEU)	Selection frequency of recovery actions (in %)				
			S1	S2	H1	H2	H3
Bushfire	0.93	18.13	0	100	0	100	0
Cyclone	0.82	47.8	0	100	5	95	0
Flooding	0.82	42.97	0	100	0	100	0

The results indicate that bushfires, characterized by localized impacts and small disruption radii, led to the highest mean resilience and the lowest CO_2 emissions. In contrast, flooding and cyclones resulted in nearly identical resilience indices and comparable emissions, despite differing in impact sensitivities. This suggests that the spatial extent of a disruption has a greater influence on overall network resilience than the intensity parameters alone.

The recovery action selection frequencies illustrate how the network adapts to each disruption type. Seaport recovery option S2 was chosen in 100% of cases, highlighting its central role in restoring capacity. On the hinterland side, H2 was selected consistently across bushfire and flooding scenarios and in most cyclone cases, with H1 appearing only under cyclones, suggesting more diversified responses under widespread impacts. However, the repeated selection of the same actions across scenarios points to a limitation: the current set of recovery options may be too narrow or idealized. This underlines the need to expand the action catalogue to better reflect real-world constraints, trade-offs, and context-dependent effectiveness.

The experiments confirm that the approach produces results consistent with scenario design and network structure, demonstrating its potential to support decision-making under uncertainty while balancing resilience and environmental sustainability. The disruption scenarios are based on simplified, synthetic data chosen to demonstrate the methodology. In reality, climate events such as bushfires typically extend across much larger areas. Thus, conclusions on resilience or emissions are illustrative, not quantitative forecasts. The primary contribution of this study is the integrated framework for optimizing recovery and sustainability in port-hinterland container networks.

4. CONCLUSION

This study introduced a two-stage optimization framework for the RG-PHCTN to evaluate and improve logistics network resilience under climate change-related disruptions. It integrates disruption modelling, Monte Carlo simulation, and recovery optimization, considering economic, temporal, and environmental objectives. Computational experiments on a synthetic Australian network showed that the framework yields plausible, interpretable results in terms of resilience, CO_2 emissions, and recovery strategies - demonstrating its strategic value for port–hinterland logistics while using stylised data to illustrate model functionality. The modular, flexible design allows recovery actions, cost factors, and emission coefficients to be adapted to local infrastructure. Its sequential MILP structure supports transparent integration of new objectives, constraints, or network features for diverse operational settings.

Future work will include a structured sensitivity analysis to assess how disruption radius and impact strength affect resilience outcomes, clarifying key drivers of resilience loss and refining model assumptions. Methodological extensions will incorporate machine learning to estimate disruption probabilities from historical climate, infrastructure, and operational data, supporting probabilistic, anticipatory planning. Further simulation enhancements, such as realistic damage propagation, time-phased recovery, and interdependent infrastructure, will increase model fidelity. To enable real-world deployment, the synthetic network will be replaced with infrastructure derived from open data sources such as Open Street Map, allowing for location-specific risk and resilience assessments. This will empower stakeholders to simulate, compare, and prepare recovery strategies for actual network layouts and regional hazards. With these developments, RG-PHCTN becomes a practical decision-support tool for sustainable, climate-resilient logistics, contributing to broader goals of low-carbon and adaptive infrastructure in an era of growing environmental uncertainty.

ACKNOWLEDGEMENTS

This research was supported by the 2024 Australia-Germany Joint Research Cooperation Scheme, a collaborative initiative between Universities Australia and the German Academic Exchange Service (DAAD).

REFERENCES

Becker A, Acciaro M, Asariotis R, Cabrera E, Cretegny L, Crist P, ... & Velegrakis AF (2018) Implications of climate change for shipping and ports: Effects on maritime infrastructure, transport costs and operations. WIREs Climate Change, 9(2), e508.

Bureau of Infrastructure and Transport Research Economics (2023) Australian Infrastructure and Transport Statistics – Yearbook 2023. Department of Infrastructure, Transport, Regional Development, Communications and the Arts.

Chen H, Cullinane K & Liu N (2017) Developing a model for measuring the resilience of a port-hinterland container transportation network. Transportation Research Part E: Logistics and Transportation Review, 97, 282–301.

Chen L & Miller-Hooks E (2012) Resilience: An Indicator of Recovery Capability in Intermodal Freight Transport. Transportation Science, Volume 46, No. 1.

Liu P, Wang C, Xie J, Mu D & Lim MK (2021) Towards green port-hinterland transportation: Coordinating railway and road infrastructure in Shandong Province, China, Transportation Research Part D: Transport and Environment, Volume 94

Nair R, Avetisyan H & Miller-Hooks E (2010) Resilience framework for ports and other intermodal components. Transportation Research Record: Journal of the Transportation Research Board, 2166(1), 54-65.

Notteboom T, Pallis A & Rodrigue J-P (2022) Port hinterlands, regionalization and corridors. In Port Economics, Management and Policy. Routledge.

Safe to Work (2025) Port Hedland shuttered as tropical cyclone becomes severe.

Sims R & Canadell P (2024) State of the Climate 2024: Australia is enduring harsher fire seasons, more ocean heatwaves and sea level rise. The Conversation.

Tian Z, Jiang F, Zhang Y, Mahmoud H, Lu X, Luo M, Guo J & Guo W (2024) Assessing seaport disruption under tropical cyclones using influence diagram and physics-based modeling. Transportation Research Part D: Transport and Environment, 132, 104237.

U.S. Bureau of Transportation Statistics (2025) Container / TEU.

